M&C 2017 - International Conference on Mathematics & Computational Methods Applied to Nuclear Science & Engineering, Jeju, Korea, April 16-20, 2017, on USB (2017)

Linear Diffusion-Synthetic Acceleration with Voids

Jijie Lou, Jim E. Morel

Department of Nuclear Engineering, Texas A&M University, College Station, TX 77843
loujijie1991@tamu.edu, morel@tamu.edu

Abstract - *Diffusion-synthetic acceleration (DSA) has been widely used for accelerating the source iteration process for the S_N equations. However, challenges arise when treating problems with voids and problems with large discontinuities in cross section. A non-local tensor diffusion theory was derived by Morel [1, 2] that provides non-zero diffusion coefficients in voids or near voids. In the current work, we use this theory to generate diffusion coefficients for linear DSA. The periodical horizontal interface problem is used to test the effectiveness of DSA with non-local diffusion coefficients. The method is also applied to problem with a void embedded in material.*

I. INTRODUCTION

The main purpose of this paper is to define a linear diffusion-synthetic acceleration (DSA) scheme for the S_N equations applicable to problems with voids. There are two difficulties that immediately present themselves in this regard. The first is that the standard diffusion coefficient is unbounded in a void. We avoid this difficulty by using a nonlocal tensor diffusion (NTD) theory originally developed by Morel [1, 2] for radiative transfer. This theory was later derived for neutronics by Trahan and Larsen [3]. This theory produces a bounded diffusion tensor at each point in the geometry that depends upon the entire distribution of cross sections throughout the geometry rather than the cross section at each point. In principle, voids can be treated in DSA schemes simply by using a very large diffusion coefficient in the void, but it is not at all clear how large the coefficient should be, and even if they lead to effective acceleration, unnecessarily large values of the diffusion coefficient can lead to an ill-conditioned diffusion matrix.

The second difficulty is that large discontinuities in cross section can significantly degrade the effectiveness of DSA [4, 5]. However, it is not clear to us that the model problems used in these references are sufficiently relevant to the problems of interest to us. In particular, we are interested in problems with voids embedded in materials with moderate cross sections. Under these conditions, one can expect to have optically-thin cells everywhere. Neutronics calculations largely fall into this category. This is in contrast to radiative transfer problems in the high energy density regime, which have optically-thin regions together with optically-thick regions that are too thick to be resolved on a sub-mean-free-path basis by the spatial mesh. Thus here we define our own set of model problems for testing the effectiveness of DSA with embedded voids. Our preliminary computational results indicate that acceptable degradation of DSA occurs as long as the cells in the optically-thick region are optically thin. This is a very encouraging result.

Schunert, et al., [6] have developed a nonlinear diffusion acceleration scheme for S_N calculations. They similarly used Morel's NTD theory in their scheme. Nonetheless, their study and our present study are complimentary for a variety of reasons.

The remainder of this paper is organized as follows. First we present the method for generating nonlocal diffusion tensors. Next we describe our model problems. Our computational results are then presented, followed by conclusions and recommendations for future work.

II. NONLOCAL DIFFUSION COEFFICIENTS

The NTD theory previously referred to provides a tensor at each point in a transport domain that depends upon the cross section distribution throughout the domain rather than the local cross section at each point [1, 2]. More specifically, to obtain the diffusion tensor, one first solves the following transport equation on the spatial domain of interest:

$$\overrightarrow{\Omega} \cdot \overrightarrow{\nabla} \tilde{\psi} + \sigma_t \tilde{\psi} = \frac{1}{4\pi} \quad , \tag{1}$$

where $\overrightarrow{\Omega}$ is the direction of neutron propogation, σ_t is the standard macroscopic total cross section associated with the transport domain, and $\tilde{\psi}$ is the angular flux solution to this problem, which is in general related to the real problem in terms of the problem domain and the definition of σ_t on that domain. Given the solution to Eq. (1), the diffusion tensor is simply given by the "pressure" tensor associated with that solution:

$$D_{ij} = \int_{4\pi} \overrightarrow{\Omega}_i \overrightarrow{\Omega}_j \tilde{\psi} \, d\Omega \quad . \tag{2}$$

And the current can be calculated by the following equations:

$$\begin{aligned} \overrightarrow{J} &= -D \cdot \overrightarrow{\nabla} \phi \quad , \\ J_i &= -\sum_{j=1}^{3} D_{ij} \frac{\partial \phi}{\partial x_j} \quad . \end{aligned} \tag{3}$$

The boundary conditions that should be used for Eq. (1) are not necessarily those of the original problem. The latter can always be used, but in some instances, it has been found that improved results can be obtained by replacing the true conditions with reflective conditions. Using reflective conditions ensures that the standard scalar diffusion coefficient is obtained in a homogeneous material, but using vacuum conditions ensures that the diffusion coefficient is bounded even in a pure

void. We partially address the question of boundary conditions in our computations. Note that Eq. (1) describes a purely absorbing medium and thus requires a single transport sweep (neglecting implicit reflective or periodic boundary conditions) to be solved. This seems like a reasonable amount of work to obtain the diffusion tensor relative to the total amount of work required to solve a general physical problem of interest.

III. COMPUTATIONAL RESULTS

The equations to be solved for the DSA calculations are given below:

$$\begin{aligned} \overrightarrow{\Omega}_m \cdot \overrightarrow{\nabla} \psi_m^{l+1/2} + \sigma_t \psi_m^{l+1/2} &= \frac{\sigma_s \phi^l}{4\pi} \quad , \\ \phi^{l+1/2} &= \sum_{m=1}^{M} w_m \psi_m^{l+1/2} \quad , \\ -\overrightarrow{\nabla} \cdot D \cdot \overrightarrow{\nabla} \delta\phi^{l+1/2} + \sigma_a \delta\phi^{l+1/2} &= \sigma_s(\phi^{l+1/2} - \phi^l) \quad , \\ \phi^{l+1} &= \phi^{l+1/2} + \delta\phi^{l+1/2} \quad . \end{aligned} \tag{4}$$

1. Characterizations of the Problems

There are two geometric configurations for our calculations given in Figs. 1 and 2: one is similar to the periodic horizontal interface (PHI) configuration [4] and the other is a configuration with a single embedded void.

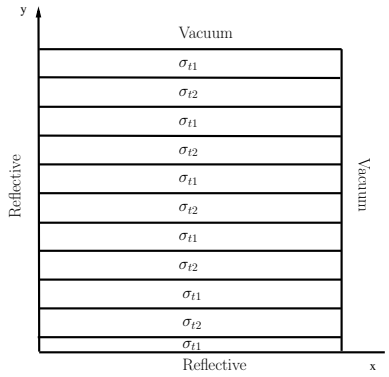

Fig. 1: The PHI-like configuration

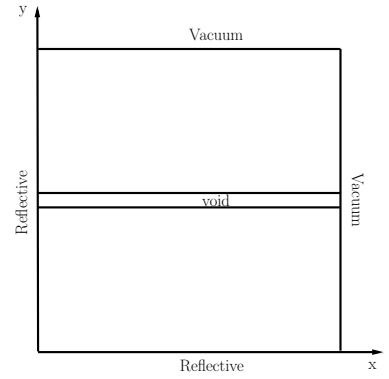

Fig. 2: The configuration with an embedded void

The PHI configuration is often used in the literature to test the effectiveness of the acceleration for heterogeneous configurations. The original PHI configuration consists of horizontal stripes of alternating materials with $\sigma_{t2} = 1/\sigma_{t1}$ [4]. It has been found that the effectiveness of DSA degrades as σ_{t1} approaches zero [4, 5]. Our PHI-like configuration, shown in Fig. 1, consists of alternating 2-cm-thick layers. The dimensions of the whole geometry are 21 cm × 21 cm. The left and bottom boundary conditions are reflective, and the top and right boundary conditions are vacuum for Eq. (4). For Eq. (1) either the same boundary conditions are used or reflective conditions are used everywhere. The value of σ_{t1} is given as 10 cm^{-1}, while $\sigma_{t2} = \tau\sigma_{t1}$ with the values of τ chosen as 10^{-1}, 10^{-2}, 10^{-3}, 10^{-4}, 10^{-5}, respectively. The scattering ratios c are chosen as 1 and 0.99, respectively.

We also have a test configuration with a void embedded in a thick material. The same dimensions and boundary conditions as the PHI-like configuration are employed here. There is a 1-cm-thick void channel in the center. The total cross section of the material is given as 10 cm^{-1}. The scattering ratios are chosen as 0.9, 0.99, 0.999, 0.9999 and 1, respectively.

The diamond difference scheme is used to spatially discretize the Eq. (4). A weighted-diamond difference scheme is used to solve Eq. (1). This latter scheme is equivalent to the step characteristics method in 1D slabs. Gauss-Chebyshev S_8 quadratures are used for all calculations. The cell thicknesses throughout each problem (Eqs. (1) and (4)) are chosen as 10, 1 and 0.1 mean free paths (mfp) measured with respect to the cross section in the thick materials. The algebraic multigrid [7] method is used to solve the diamond-difference-consistent DSA diffusion equations. Calculations are performed for Eq. (4) with random values for the initial scalar fluxes. The spectral radius is calculated as $\rho = \|\phi^{l+1}\|/\|\phi^l\|$. The iteration process is terminated when $|\rho^{l+1} - \rho^l| \leq 10^{-5}$. The same boundary conditions are used to solve Eqs. (1) and (4) unless otherwise stated.

2. Results for the PHI-like Configuration

A. Diffusion Tensor Plots

The diffusion tensor elements D_{xx}, D_{yy}, and D_{xy}, obtained with a cell thickness of 1 mfp and $\tau = 10^{-3}$, are plotted in Fig. 3. For comparison, the diagonal elements D_{xx}, D_{yy} at $x = 10.5$ cm are also plotted with different cell thicknesses in Fig. 4. It is expected that the values of D_{xx} are larger than D_{yy} in the thin materials. The values of D_{xy} are almost 0 everywhere except on the material interfaces. We set D_{xy} to zero in all our calculations for Eq. (4), which yields a diagonal diffusion tensor.

B. Vacuum and Reflective Conditions for Eq. (1)

This set of calculation has reflective conditions on the left and bottom boundaries, and vacuum conditions on the right and top boundaries for both Eqs. (1) and (4). The calculated spectral radii for DSA using either the local diffusion coefficients (LDC) or the diagonal NTD with $c = 1$ are listed in Table I, along with the spectral radii from source iteration (SI). From the results, we find that when increasing the heterogeneity, the spectral radii are essentially constant for SI but

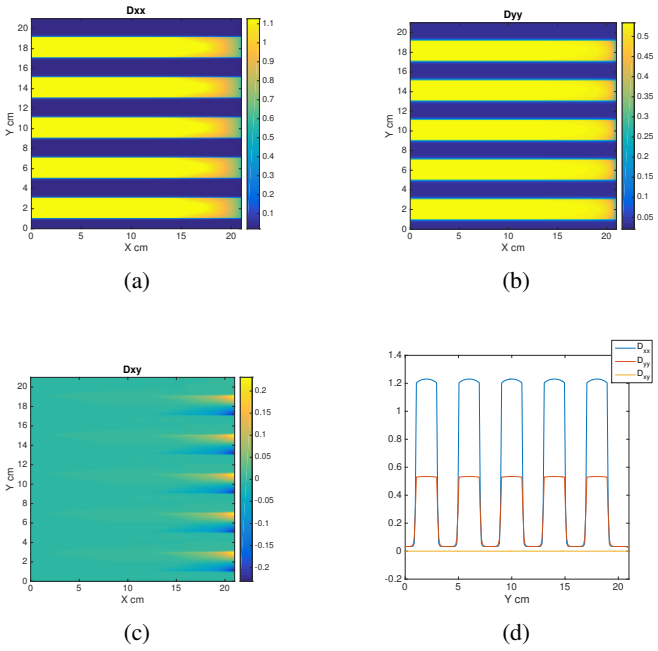

Fig. 3: The diffusion tensor calculated for the PHI-like configuration with a cell thickness of 1 mfp and $\tau = 10^{-3}$.

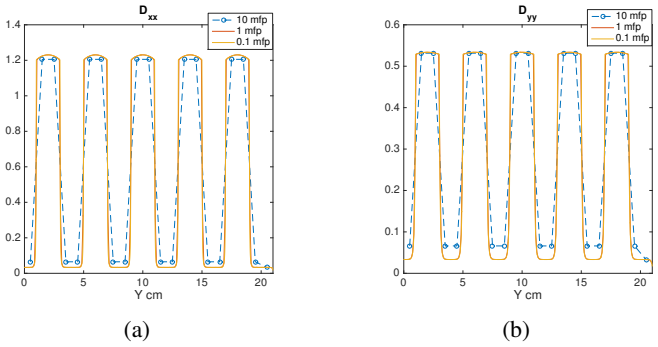

Fig. 4: The diagonal elements of the diffusion tensor calculated for the PHI-like configuration with different cell thicknesses and $\tau = 10^{-3}$.

increase for DSA. For SI, the spectral radii are close to 0.999, and the results change slightly with the cell thicknesses ≤ 1 mfp. For LDC, the spectral radius is roughly around 0.793 with a cell thickness of 10 mfp and $\sigma_{t2} = 10^{-1}$. Decreasing the cell thicknesses to 1 mfp gives spectral radius to 0.689. Further decreasing the cell thicknesses yields stagnation in spectra radii. For more heterogeneous cases, reducing the cell thicknesses can slightly reduce the spectral radii. However, in those cases, the spectral radii are about 0.95. For NDT, DSA goes on unstable with a cell thickness of 10 mfp. However, with the cell thicknesses ≤ 1 mfp, NTD gives much better results compared to LDC. As mentioned before, in neutronics calculations, all cells can usually be made thin. In contrast to LDC, there is slight increase in the spectral radii for NTD with decrease in the cell thicknesses from 1 mfp to 0.1 mfp. Further increasing the heterogeneity, there is negligible increase in the spectra radii. Similar results are observed in Table II with a cell thickness of 1 mfp and $c = 0.99$.

C. Reflective Conditions for Eq. (1)

This set of calculation has reflective boundary conditions on all boundaries for Eq. (1) but still has the same boundary conditions used in the previous section for Eq. (4). In the previous calculation, we used the same boundary conditions for Eqs. (1) and (4). However in the derivation of non-local tensor diffusion theory, we have assumed infinite medium and neglected the boundary term. Here we also explored the effect of boundary conditions used for generating the diffusion tensor. The spectral radii, obtained with the diagonal NTD generated from reflective boundary conditions and a cell thickness of 1 mfp, are listed in Table III. Slight increase in the spectral radii is observed compared to the results in the previous section.

3. Results for the Configuration with an Embedded Void

A. Diffusion Tensor Plots

The diffusion tensor elements D_{xx}, D_{yy}, D_{xy}, obtained with a cell thickness of 1 mfp for the configuration with an embedded void, are plotted in Fig. 5. It is observed that the values of the diagonal elements in the void are about half of the values in the thin materials in Fig. 3. This is related to the fact that the diffusion coefficients in a void surrounded by the thick material are related to the dimensions of the void.

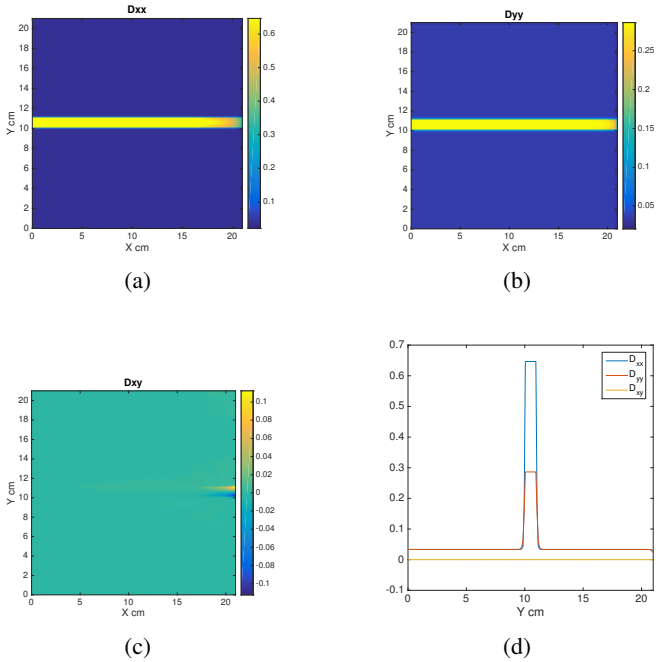

Fig. 5: The diffusion tensor calculated for the configuration with an embedded void with 1-mfp-thick cells.

τ	SI			LDC			NTD		
	10 mfp	1 mfp	0.1 mfp	10 mfp	1 mfp	0.1 mfp	10 mfp	1 mfp	0.1 mfp
1.0E-02	0.99894	0.99927	0.99927	0.79309	0.68851	0.68852	1.16897	0.65821	0.67484
1.0E-03	0.99882	0.99918	0.99918	0.92481	0.92091	0.87093	1.48523	0.68945	0.70348
1.0E-04	0.99883	0.99918	0.99917	0.97110	0.95197	0.92088	1.52010	0.69251	0.71330
1.0E-05	0.99883	0.99918	0.99917	0.97692	0.95517	0.95196	1.52402	0.69282	0.71359
1.0E-06	0.99883	0.99918	0.99997	0.97751	0.95549	0.95547	1.52441	0.69285	0.71363

TABLE I: Spectral radii for the PHI-like configuration with different cell thicknesses and $c = 1$.

τ	SI	LDC	NTD
1.0E-02	0.98927	0.59833	0.64425
1.0E-03	0.98919	0.76762	0.67572
1.0E-04	0.98918	0.83640	0.67895
1.0E-05	0.98918	0.84530	0.67928
1.0E-06	0.98918	0.84621	0.67931

TABLE II: Spectral radii for the PHI-like configuration with a cell thickness of 1 mfp and $c = 0.99$.

τ	NTD	
	c=0.99	c=1
1.0E-02	0.64427	0.65845
1.0E-03	0.67617	0.69034
1.0E-04	0.67947	0.69362
1.0E-05	0.67980	0.69395
1.0E-06	0.67984	0.69398

TABLE III: Spectral radii for the PHI-like configuration using diagonal NTD generated from reflective boundary conditions with a cell thickness of 1 mfp.

B. Calculated Set for Spectral Radii

The spectral radii, obtained with different scattering ratios and cell thicknesses for SI and DSA with NTD, are given in Table IV.

As expected, the spectral radii increase with the scattering ratios. For SI, the same results are observed as for the PHI-like problem: the spectral radii are essentially stable and close to c with different cell thicknesses. For NTD, one encouraging result is that it works with thick cells. For cases $c = 0.9$ and 0.99, the spectral radii decrease with cell thicknesses, while further increasing c, the spectral radii first decrease then increase with cell thicknesses. Although the reason for such behavior seems unclear, the point here is that NTD works well for the configuration with a single embedded void, giving spectral radii far less than c.

IV. CONCLUSIONS

In this paper, we used a PHI-like configuration and an embedded void configuration to test the use of NTD theory for linear DSA. In the PHI-like configuration, NTD yields instability with thick cells, but performs better than LDC with good mesh resolution. The performance of NTD in the void configuration is better than it is for the PHI-configuration, and remains stable with thick cells. Our result suggests that NTD will be effective in typical neutronics applications with near-voids or voids. Finally, our results suggests that using the vacuum boundary conditions for NTD generation is a better option than the reflective conditions.

V. FUTURE WORK

In the future, we would like to apply this method to practical problems. We would also like to investigate using a more refined mesh for calculating the diffusion tensor and mapping it to the problem mesh. A further detailed analysis should be performed to understand why NTD fails for the PHI-like configuration with thick cells. Finally it would be useful to test the use of NTD for DSA preconditioning in conjunction with a Krylov solver, particularly for cases where it is unstable.

VI. ACKNOWLEDGMENTS

This material is based upon work supported by the Department of Energy, National Nuclear Security Administration, under Award Number(s) DE-NA0002376, and by the Department of Energy, Battelle Energy Alliance, LLC, under Award Number(s) DE-AC07-05ID14517.

REFERENCES

1. J. MOREL, "A Nonlocal Tensor Diffusion Theory," Tech. Rep. LA-UR-07-5257, Los Alamos National Laboratory (2007).
2. J. MOREL, J. WARSA, and K. BUDGE, "Alternative Generation of Nonlocal Diffusion Tensors," Tech. Rep. LA-UR-10-08285, Los Alamos National Laboratory (2010).
3. T. J. TRAHAN and E. W. LARSEN, "3-D Anisotropic Neutron Diffusion in Optically Thick Media with Optically Thin Channels," in "Proc. Int. Conf. on Math. and Comp. Methods Applied to Nuclear Science and Eng. (M&C 2011)," American Nuclear Society, Rio de Janeiro, RJ, Brazil, May 8-12, 2011 (2011).
4. Y. AZMY, "Unconditionally Stable and Robust Adjacent-Cell Diffusive Preconditioning of Weighted-Difference Particle Transport Methods is Impossible," *Journal of Computational Physics*, **182**, 213–233 (2002).
5. J. S. WARSA, T. A. WAREING, and J. E. MOREL, "Krylov Iterative Methods and the Degraded Effectiveness

c	SI			NTD		
	10 mfp	1 mfp	0.1 mfp	10 mfp	1 mfp	0.1 mfp
0.9	0.89977	0.89977	0.89977	0.35518	0.49221	0.51321
0.99	0.98975	0.98975	0.98975	0.54070	0.57868	0.59617
0.999	0.99875	0.99875	0.99875	0.62569	0.58869	0.60568
0.9999	0.99965	0.99965	0.99965	0.64349	0.58992	0.60704
1	0.99975	0.99975	0.99975	0.64697	0.58954	0.60654

TABLE IV: Spectral radii for the configuration with an embedded void with different cell thicknesses and c values.

of Diffusion Synthetic Acceleration for Multidimensional S_n Calculations in Problems with Material Discontinuities," *Nuclear Science and Engineering*, **147**, 218–248 (2004).

6. S. SCHUNERT, H. HAMMER, J. LOU, Y. WANG, J. ORTENSI, F. GLEICHER, B. BAKER, M. DEHART, and R. MARTINEAU, "Using Directional Diffusion Coefficients for Nonlinear Diffusion Acceleration of the First Order S_N Equations in Near-Void Regions," in "Transactions of the American Nuclear Society, Vol. 115," Las Vegas, NV, November 6-10, 2016 (2016).
7. Y. NOTAY, "AGMG software and documentation," Http://homepages.ulb.ac.be/ ynotay/AGMG.